Acta Pharmaceutica Sinica B 2023;13(5):2039–2055

Chinese Pharmaceutical Association
Institute of Materia Medica, Chinese Academy of Medical Sciences

Acta Pharmaceutica Sinica B

www.elsevier.com/locate/apsb
www.sciencedirect.com

ORIGINAL ARTICLE

The host-targeting compound peruvoside has a broad-spectrum antiviral activity against positive-sense RNA viruses

Kan Xing Wu[e,†], Thinesshwary Yogarajah[a,c,†], Marcus Wing Choy Loe[a], Parveen Kaur[a], Regina Ching Hua Lee[a], Chee Keng Mok[f], Yi Hao Wong[f], Patchara Phuektes[b], Li Sze Yeo[a], Vincent T.K. Chow[a,c], Yong Wah Tan[d], Justin Jang Hann Chu[a,b,d,f,*]

[a]*Department of Microbiology and Immunology, Yong Loo Lin School of Medicine, National University Health System, National University of Singapore, Singapore 117597, Singapore*
[b]*Department of Pathobiology, Faculty of Veterinary Medicine, Khonkaen University, Khonkaen 40002, Thailand*
[c]*Infectious Disease Programme, Yong Loo Lin School of Medicine, National University of Singapore, Singapore 117597, Singapore*
[d]*Institute of Molecular and Cell Biology, Agency for Science, Technology and Research (A*STAR), Singapore 138648, Singapore*
[e]*Lee Kong Chian School of Medicine, Nanyang Technological University, Singapore 308232, Singapore*
[f]*NUSMed Biosafety Level 3 Core Facility, Yong Loo Lin School of Medicine, National University of Singapore, Singapore 117599, Singapore*

Received 31 October 2022; received in revised form 22 February 2023; accepted 2 March 2023

KEY WORDS

Positive-sense RNA viruses;
Peruvoside;
Antiviral;
CDKI signaling;
Viral factories;
Calcium efflux;
Broad-spectrum;

Abstract Positive-sense RNA viruses modify intracellular calcium stores, endoplasmic reticulum and Golgi apparatus (Golgi) to generate membranous replication organelles known as viral factories. Viral factories provide a conducive and substantial enclave for essential virus replication *via* concentrating necessary cellular factors and viral proteins in proximity. Here, we identified the vital role of a broad-spectrum antiviral, peruvoside in limiting the formation of viral factories. Mechanistically, we revealed the pleiotropic cellular effect of Src and PLC kinase signaling *via* cyclin-dependent kinase 1 signaling leads to Golgi-specific brefeldin A-resistance guanine nucleotide exchange factor 1 (GBF1) phosphorylation and Golgi vesiculation by peruvoside treatment. The ramification of GBF1 phosphorylation fosters

*Corresponding author. Tel.: +65 65163278.
E-mail address: miccjh@nus.edu.sg (Justin Jang Hann Chu).
[†]These authors made equal contributions to this work.
Peer review under the responsibility of Chinese Pharmaceutical Association and Institute of Materia Medica, Chinese Academy of Medical Sciences.

https://doi.org/10.1016/j.apsb.2023.03.015

Golgi apparatus

GBF1 deprivation consequentially activating downstream antiviral signaling by dampening viral factories formation. Further investigation showed signaling of ERK1/2 pathway *via* cyclin-dependent kinase 1 activation leading to GBF1 phosphorylation at Threonine 1337 (T1337). We also showed 100% of protection in peruvoside-treated mouse model with a significant reduction in viral titre and without measurable cytotoxicity in serum. These findings highlight the importance of dissecting the broad-spectrum antiviral therapeutics mechanism and pave the way for consideration of peruvoside, host-directed antivirals for positive-sense RNA virus-mediated disease, in the interim where no vaccine is available.

1. Introduction

Positive-sense RNA viruses are known to induce extensive rearrangements of intracellular membranes from endoplasmic reticulum (ER) and Golgi apparatus into clusters of double membrane vesicles (DMVs) or convoluted membranes that serve as vital sites for viral genome replication, polyprotein processing and formation of progeny virions[1,2]. Though studies have investigated antiviral compounds targeting viral protein or viral genomes in convoluted membranes or cytoplasm of cells, not many antivirals are designed to target host factors modulating viral replication due to off-target effects of compounds. For example, the pandemic of SARS-CoV-2[3,4] has motivated clinicians and scientists to identify suitable drug treatments against this virus owing to the fact that most drugs are direct-acting compounds with specific inhibitory activity against viruses. Hence our goal is to minimize the development of antiviral drug combinations, and to identify a broad-spectrum inhibitor with a characterized antiviral mechanism.

Plant-derived saponin glycosides have been routinely prescribed to treat cardiac failure and arrhythmia *e.g.*, peruvoside, digitoxigenin, lanatoside C and ouabain. Basically, these compounds function by exerting a positive inotropic effect on cardiac muscle cells, raising intracellular calcium concentration to increase muscle contractility. In addition, they are specific inhibitors of the sodium potassium pump (Na^+/K^+ ATPase) located at the plasma membrane. The Na^+/K^+ ATPase actively pumps out sodium ions while bringing in potassium ions to maintain resting transmembrane potential in cells. In the classical 'ionic' pathway, the binding of glycosides at the extracellular binding site of the Na^+/K^+ ATPase α-subunit results in a complete loss of pump activity and an eventual increase in cytosolic sodium[5]. This would then alter the function of the Na^+/Ca^{2+} exchanger, resulting in an increase in intracellular free calcium (Ca^{2+})[6]. Recent studies and the discovery of endogenous steroids, have led to the proposal of a pathway reminiscent of ligand-receptor signaling cascades[7] involving Na^+/K^+ ATPase associating with the tyrosine kinase, Src, in a signaling complex with epidermal growth receptor[8]. Glycosides binding of Na^+/K^+ ATPase activates Src, which then transactivates epidermal growth receptor to trigger a series of complex signaling cascades including Ras-mediated Raf-ERK1/2 kinase cascade to trigger gene expression changes in the cell[9,10]. Low dose stimulation by steroids can also generate intracellular Ca^{2+} oscillations through activated L-type voltage-gated channels, PLC activation and consequently, IP_3-stimulated release of intracellular Ca^{2+} stores[11]. For example, one of these compounds, digitoxin, exhibits antiviral activities against RNA virus (influenza virus)[12] and DNA viruses such as herpes simplex virus (HSV1)[13,14] and human cytomegalovirus[15]. However, the mechanism of action as an antiviral remains largely unknown and should be deliberated.

In this study, we discovered that intracellular calcium flux triggered by peruvoside is essential to its broad-spectrum antiviral activities. Closer interrogation revealed new contributing roles for both extracellular Ca^{2+} influx and intracellular Ca^{2+} store release. Upon peruvoside treatment, we disclosed that cyclin-dependent kinase 1 (CDK1) signaling caused Golgi-specific brefeldin A-resistance guanine nucleotide exchange factor 1 (GBF1) phosphorylation which in-turn leads to Golgi vesiculation, as an important role for its antiviral activity. Peruvoside has hitherto not been reported as an antiviral drug, hence indicating it is distinct in exhibiting a common inhibitory mechanism consistently observed in positive-sense RNA viruses from four virus families including Picornaviridae, Togaviridae, Flaviviridae and Coronaviridae. Using enterovirus A71 (EV-A71), chikungunya virus (CHIKV), Zika virus (ZIKV), dengue virus 2 (DENV2), severe acute respiratory syndrome coronavirus 2 (SARS-CoV-2), murine hepatitis virus (MHV) as well as a DNA virus (HSV1) and two negative-sense RNA virus (H1N1 and hRSV), we affirm that peruvoside exerts broad-spectrum inhibition of virus replication across distant families of positive-sense RNA, negative-sense RNA and even DNA viruses *via* this distinctive pathway of GBF1 deprivation and limiting viral factories formation.

2. Materials and methods

2.1. Cell cultures and viruses

All cell lines used were obtained from American Type Culture Collection (ATCC) and collaborator as described in Supporting Information Table S1. Cells were cultured in media supplemented with 10% fetal calf serum (FCS, PAA Laboratories). All viruses were propagated in appropriate cell lines in media supplemented with 2% FCS. All live cultures in this study were incubated in a humidified incubator under 5% CO_2 at 37 °C. Detailed information on strains and cell lines used can be found in Supporting Information.

Enteroviruses (EV-A71, CV-A16, CV-A6 and Echovirus 7) and HSV1 propagation and infection assays were performed in human rhabdomyosarcoma (RD) cells. CHIKV was propagated in cell clone C6/36 (*Aedes albopictus*); inhibition assays were performed on SJCRH30 cells and plaque assays on baby hamster kidney (BHK-21) cells. ZIKV and DENV2 were propagated in C6/36;

inhibition assays were performed on human hepatocarcinoma (Huh7) cells and plaque assays on BHK-21 cells. MHV were propagated and inhibition assay as well as plaque assay performed in *Mus musculus* hepatocyte cells (H2.35) cells. SARS-CoV-2 were propagated and inhibition assay as well as plaque assay performed in Vero E6 cells. All SARS-CoV-2 work was performed in a biosafety level 3 (BSL-3) laboratory and all protocols were approved by the BSL-3 Biosafety Committee and Institutional Biosafety Committee of the National University of Singapore (protocol No. 2020-00574). Influenza virus H1N1 were propagated and inhibition assay as well as plaque assay performed in MDCK cells. HRSV were propagated and inhibition assay as well as $TCID_{50}$ assay[16] performed in A549 cells. All virus strains were presented in Supporting Information Table S2.

2.2. *In vitro virus infection*

Generally, media overlaying seeded monolayers of host cells was removed before inoculation with virus. Virus adsorption was allowed to take place for 1 h for enteroviruses, HSV1, ZIKV, DENV2, SARS-CoV-2 and hRSV, and 1.5 h for CHIKV, and 2 h for MHV. After adsorption period, the inoculum was removed, and monolayers were washed with phosphate-buffered saline (PBS) before media was replaced. Indicated times of infection (hpi) in the data excludes the adsorption period. In antiviral assays, media containing the indicated final concentrations of compounds/controls were added. Stock virus titres were determined using plaque assay for all virus, except hRSV where $TCID_{50}$ was used for virus titre determination. All virus infections were performed with the same technique unless otherwise mentioned.

2.3. *Virus quantitation*

Plaque assays for enteroviruses and HSV1 were performed for media collected at the respective experimental endpoints. Samples were serially diluted before infection of cell monolayers. After virus adsorption, an overlay media containing 0.5% agarose was added, while for H1N1 overlay media containing 0.3% agarose was added. RD cells were fixed and stained with 4% paraformaldehyde and 1% crystal violet after specific incubation periods for each virus and plaques were counted visually and expressed as plaque forming units per mL (PFU/mL). For SARS-CoV-2 Vero E6 were used while for CHIKV, ZIKV, DENV2, and MHV the overlay media used contained 1% Aquacide II (Calbiochem) instead of agarose. For hRSV $TCID_{50}$[16] was used. For relative infection experiments, samples were fixed and stained with an EV-A71 specific primary antibody for VP2 (Millipore) and a FITC-conjugated secondary antibody (Millipore). Nuclei were counterstained with 4′,6-diamidino-2-phenylindole, DAPI (MP Biomedicals). Imaging was performed using ImageXpress Micro XLS (Molecular Devices, San Jose, CA, USA) and CellProfiler was used to count number of nuclei and total number of VP2-expressing cells. Relative infection rates were obtained by dividing total number of VP2-expressing cells by the nuclei count and normalized with drug vehicle treated control.

2.4. *Cell viability assay*

Uninfected cells were treated with test compounds for 12 h in RD cells, 24 h in SJCRH30 and H2.35 cells, and 48 h for Huh7 and Vero E6 cells before replacement with fresh media containing alamarBlue™ cell viability reagent (Life Technologies) and incubated for 2 h. Readings were obtained using fluorescence detection at 570 nm (Ex)/600 nm (Em) and normalized with 0.1% DMSO-treated cells to compute relative cell viability.

2.5. *Compounds*

The screen was performed with the natural products library (BML-2865, Enzo Life Sciences, NY, USA). For downstream experiments powdered purified compounds were purchased, dissolved in dimethyl sulfoxide (DMSO, MP Biomedicals) and aliquots stored at −20 °C. Details of all compounds used in experiments are listed in Supporting Information Table S3.

2.6. *Electron microscopy*

RD cells were infected with EV-A71 at multiplicity of infection (MOI) of 10. At indicated time-points, the cultures were fixed and processed following the method described in our previous work by Low et al.[17].

2.7. *Nano-luciferase replicons*

NanoLuc (Promega) was cloned into the P1 region of a full-length EV-A71 (HFM41) infectious clone[18]. Mutagenesis of 3D C-terminal deletion was carried out based on Burns et al.[19] using In-Fusion HD cloning (Clontech). *In vitro* transcription was performed using MEGAscript T7 transcription kit (Life Technologies) and purified using RNeasy kit (Qiagen). Transcripts were checked for integrity and concentration using agarose-gel electrophoresis. 200 ng of purified-RNA transcripts were reverse-transfected into RD cells in white 96-well plates (Corning) using Dharmafect-1 (Thermo Scientific). At 4 h post-transfection, drug-containing media was added to give the final indicated concentration. Nano luciferase expression was detected using Nano-Glo Luciferase Assay System (Promega) at 12 h post-transfection using the GloMax 20/20 plate reader (Promega, Madison, WI, USA).

2.8. *Flow cytometry*

Cultured cells in 24-wells were washed twice with 1× Hanks' balanced salt solution containing 50 nmol/L peruvoside for treated cells or 0.1% DMSO for untreated cells at indicated time-points. Cells were then detached from well plates using Accutase cell detachment solution (Zuellig Pharma) containing either 50 nmol/L peruvoside for treated cells or 0.1% DMSO for untreated cells. Detached cells were incubated with Fluor-4NW Calcium Assay kit loading solution at 37 °C for 30 min, then at room temperature for an additional 30 min before running flow cytometry using Attune NxT Flow Cytometer (Life Science Institute, National University of Singapore, Singapore). Ionomycin (20 μg/mL) was used as calcium expression control. Data were analyzed using FlowJo (version 10). Data were normalized to basal level (0.1% DMSO-treated cells) of calcium signaling in cells using X mean value obtained for Fluor-4NW forward scatter against green channel side scatter.

2.9. *siRNA knockdown*

siRNAs used were purchased from Dharmacon siGENOME collection (Supporting Information Table S4) and reverse-transfected into RD cells using Dharmafect-1 (Thermo

Scientific) at a final concentration of 25 nmol/L, following recommended protocol. At 3 days post-transfection, media was removed for infection and drug treatment to be carried out as described. Non-targeting siRNA pool (NT) was used as control.

2.10. XBP1 cleavage

XBP1-specific primers were used in a PCR to check for XBP1 cleavage (spliced: 263 bp, unspliced 283 bp). Total RNA was extracted using RNeasy kit (Qiagen) and treated with DNase I (Promega) according to manufacturer's instructions. The RNA samples were then reverse using Moloney Murine Leukemia Virus Reverse Transcriptase (Promega) at 42 °C for 30 min. Generated cDNAs were amplified using PCR, Go-Taq Green Master Mix (Promega), and samples were resolved in a 2% agarose gel electrophoresis. Primers used are tabulated in Supporting Information Table S5.

2.11. Indirect immunofluorescence

Immunofluorescence imaging was performed on cells seeded onto glass coverslips. Cells were fixed with 4% paraformaldehyde at room temperature for 15 min followed by permeabilization with 0.1% Triton X-100 (Sigma−Aldrich) for 10 min at room temperature. Primary antibodies were diluted in PBS and incubated overnight at 4 °C. Secondary antibodies were incubated for 1 h at 37 °C. PBS washes were carried out between antibody stainings. The primary antibodies used were mouse anti-double-stranded RNA (dsRNA) (SCICONS), mouse anti-GM130 (BD Biosciences), rabbit anti-GM130 (Abcam), rabbit anti-GBF1 (Abcam) and rabbit anti-Calnexin (Abcam). Secondary antibodies used were goat FITC-conjugated anti-mouse antibody (Millipore) and goat rhodamine-conjugated anti-rabbit antibody (Millipore). Stained coverslips were mounted using mounting medium with DAPI (Sigma−Aldrich). Confocal microscopy was performed using Nikon A1R-Si confocal microscope at Nikon Imaging Center (Singapore Bioimaging Consortium, Singapore) and Olympus FV1000-IX81 Confocal Microscope (Confocal Microscopy Unit, National University of Singapore, Singapore). Vesiculation of the Golgi was quantified using CellProfiler (version 2.2.0) Measure granularity module with structuring element of radius 1 pixel and normalized against 0.1% DMSO-treated cells to give relative granularity[20].

2.12. Western blot

Protein lysates were obtained by direct lysis with 1× Laemmli buffer and resolved on SDS-polyacrylamide gels then blotted onto nitrocellulose membranes (Bio-Rad Laboratories). Primary antibodies used were rabbit polyclonal anti-GBF1 (Abcam), rabbit polyclonal anti-phospho-GBF1 T1337 (Takara), rabbit polyclonal phospho-(Ser/Thr) Akt Substrate (Cell Signaling), mouse monoclonal anti-ERK1 (pT202/pY204)+ERK2 (pT185/pY187) (Abcam), rabbit polyclonal anti-ERK1/2 (Promega), mouse monoclonal anti-EV-A71 (Millipore), mouse monoclonal anti-actin (Millipore), mouse anti-DENV Envelope Protein GTX629117 (Genetex), rabbit anti-ZIKV Envelope Protein DIII ZV-67 (Absolute Antibody), in-house produced mouse anti-CHIKV capsid protein, rabbit polyclonal p-PERK (Phospho-Thr 982), rabbit polyclonal anti-ATF6 and mouse anti-tubulin. Secondary antibodies used were HRP-conjugated goat anti-mouse and anti-rabbit antibodies (Millipore). Chemiluminescent reagent used was SuperSignal West Dura Extended Duration substrate (Thermo Scientific, Massachusetts, USA) and all blots were scanned with C-DiGit Blot Scanner (LI-COR Biosciences, Nebraska, USA) and band intensities were analysed with Image Studio (LI-COR Biosciences).

2.13. Plasmids and transfection

The open reading frame for GBF1 from the Kazusa collection (Promega) was cloned into pLX-V5 vector to include a C-terminal V5 tag. Cloning and mutagenesis were performed using In-Fusion HD cloning kit (Clontech). Sequence-verified clones were transfected into RD cells using jetPRIME (Polyplus-Transfection) and 5 μg/mL blasticidin (Life Technologies) was used to select stable expressing cells. Colonies of resistant cells were picked using cloning discs to obtain clonal populations of transformed cells which were then verified for expression by Western blotting.

2.14. Mouse model of EV-A71 infection

7-day-old BALB/c mice were injected intraperitoneally with virus inoculum. Mock infected mice were injected with mock-infected cell culture media. In antiviral studies, 100 μL of 0.59 mg/kg dose of peruvoside in PBS was injected intraperitoneally. Treatment was carried out daily for 1-week post infection. Survival studies were carried out for 21-days post infection. Histological analysis was carried out on mice sacrificed at 5 days post-infection. The humane endpoint was determined using a clinical scoring system. Mice were scored in 4 categories for symptoms observed during the 21-day survival study. Activity: 0 normal, 1 lethargy/abnormal posture, 2 huddled/inactive, 3 moribund/seizure; Breathing: 0 normal, 1 rapid/shallow, 2 rapid abdominal, 3 blue; Movement: 0 normal, 1 weakness, incoordination, 2 single limb dragging/paralysis, 3 multiple limb dragging/paralysis; Body weight: 0 normal, 1 loss of 5% over 24 h, 2 loss of more than 15% or up to 10% in 24 h, 3 loss of more than 10% over 24 h or 20% in total. A total of 6 or more points accumulated across all categories was determined as a humane endpoint and mice with such a score was euthanized.

2.15. LDH assay

Collected whole murine blood was left to clot at room temperature for 10 min before centrifugation at 2500 × *g* for 15 min at 4 °C to isolate serum. LDH levels was obtained with serum using LDH Cytotoxicity Assay Kit (Abcam) according to manufacturer's instructions.

2.16. Ethics statement

Animal care and housing were provided in accordance with the National Advisory Committee for Laboratory Animal Research (NACLAR) Guidelines (Guidelines on the Care and Use of Animals for Scientific Purposes). Experiments with mice were designed and approved under protocol 088/10 by National University of Singapore Institutional Animal Care & Use Committee (IACUC) based on NACLAR guidelines.

2.17. Statistical analyses

GraphPad Prism 6 was used for Kaplan−Meier survival analysis. Student's *t*-test for unpaired, two-tailed tests for significance was

performed on Microsoft Excel and one-way ANOVA with Dunnett's post-test was performed in GraphPad prism 6. For studies involving heterogeneous selection, we conducted two-way analyses of variance (ANOVAs) using GraphPad prims 6 and $P \leq 0.05$ was considered significant.

3. Results

3.1. *Peruvoside is a broad-spectrum and potent antiviral*

A prominent single-dose (10 μmol/L) of distinct natural products treatment *via* indirect immunofluorescence cell-based screens were performed using EV-A71 strain H (ATCC) as representative for positive-sense RNA viruses. The 502-compound flavonoid derivatives library (BML-2865, Enzo Life Sciences) encompassed diverse classes of natural products including terpenoids, alkaloids, coumarins, macrolides, flavones and their synthetic derivatives. Our primary screens analyses revealed three glycosides (*i.e.*, ouabain, bufalin and peruvoside) among the top 20 non-cytotoxic inhibitors of EV-A71. These three hit compounds, all glycosides were selected for further evaluations by viral plaque reduction assays, and we observed notable dose-dependent inhibition at nanomolar concentrations that was consistent with immunofluorescence assays (Fig. 1). We showed that ouabain at 50 nmol/L yield a 0.5-$\log_{10}$ units reduction and at 100 nmol/L yield about 2-$\log_{10}$ units reduction in EV-A71 viral titre. We found that bufalin at 50 nmol/L yield a 3.5-$\log_{10}$ units reduction and at 100 nmol/L yield a 3-$\log_{10}$ units reduction in EV-A71 viral titre. Our analysis revealed that peruvoside was the most efficient inhibitor among these compounds. This is because at 50 nmol/L of peruvoside treatment, EV-A71 viral titre showed about 4-$\log_{10}$ units reduction and at 100 nmol/L EV-A71 were undetected *via* plaque assay. These compounds also showed negligible adverse effects on the cell viability of human rhabdomyosarcoma at all the concentrations tested. Peruvoside was selected for subsequent studies due to its stronger inhibition of EV-A71 strain H replication, and its functional activity as it has not been reported as an antiviral compound to date.

To explore the broad-spectrum of peruvoside's antiviral activity, cells treated with peruvoside were infected with EV-A71 strain HFM41, coxsackievirus A6 (CV-A6) and A16 (CV-A16) from *Enterovirus A* genus and Echovirus 7 strain Wallace from *Enterovirus B*. Dose-dependent inhibition was evident at tested concentrations of 20 to 100 nmol/L (Supporting Information Fig. S1A−S1D) with no observable cytotoxicity in the tested concentration (Table 1). EC_{50} (effective concentration to reduce virus titer to 50%) were calculated for tested viruses; EV-A71, CV-A6, CV-A16, and Echo-7 showed EC_{50} of 18.63, 4.79, 24.52 and 1.62 nmol/L respectively (Table 1). The results suggest peruvoside demonstrated a broad-acting inhibition of enteroviruses spanning *Enterovirus A* and *B* species.

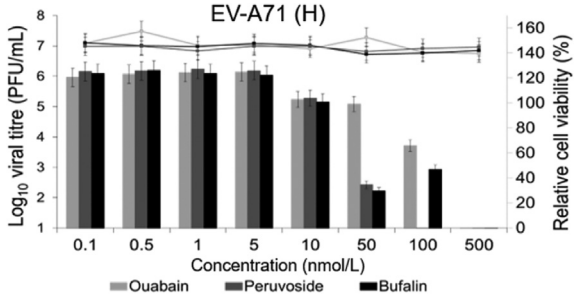

Figure 1 Peruvoside inhibits the replication of EV-A71. Viral plaque assay was performed to determine infectious titre of EV-A71 after treatment with indicated doses of peruvoside, ouabain and bufalin. Cell viability of uninfected RD cells treated with the same doses of compounds for 12 h was determined using alamarBlue and expressed as a percentage relative to 0.1% DMSO-treated cells. Bars represent viral titre and lines represent relative cell viability. Error bars indicate standard deviation (SD), $n = 3$.

Since peruvoside was active against two genera of picornaviruses, the same experiment was performed for other families of selected positive-strand RNA viruses (Fig. S1E−S1L), namely Togaviridae (CHIKV), Flaviviridae (ZIKV and DENV2), Coronaviridae (SARS-CoV-2 and MHV), a double-stranded DNA virus from Herpesviridae (HSV1), and two negative-sense single stranded RNA virus from Orthomyxoviridae (H1N1) and Paramyxoviridae (hRSV). Cell viability was also assessed as the cell lines and treatment durations were different for the viruses tested and showed no observable cytotoxicity up to 100 nmol/L tested concentration. We showed that peruvoside treatment reduced viral titres in a dosage-dependent manner for all tested viruses similar to picornaviruses (Fig. S1E−S1L). EC_{50} for mosquito-borne viruses; CHIKV, ZIKV and DENV2 infected cells were 10.14, 14.55, and 18.01 nmol/L, respectively, while EC_{50} for coronaviruses; SARS-CoV-2 and MHV were 14.09 and 20.83 nmol/L, respectively. Peruvoside treated double-stranded DNA virus; HSV1 infected cells showed EC_{50} at 19.25 nmol/L (Table 1), while peruvoside treated negative-sense RNA viruses; H1N1 and hRSV showed EC_{50} at 51.39 and 45.24 nmol/L, respectively. These results demonstrate the broad-spectrum antiviral activity of peruvoside which extends across four families of positive-sense RNA viruses, Picornaviridae, Coronaviridae, Togaviridae and Flaviviridae, one family of DNA virus, Herpesviridae and two family of single-stranded Negative-sense RNA virus, Orthomyxoviridae and Paramyxoviridae.

3.2. *Peruvoside reduces mortality in EV-A71-infected mice*

We demonstrate the *in vivo* efficacy of peruvoside using our established 1-week-old BALB/c murine model of EV-A71 (HFM41) infection[21]. Neonatal mice were infected *via* intraperitoneal (i.p.) injection of 1×10^5 PFU EV-A71. Infected neonates developed symptoms and reached clinical end-point within 10-days post-infection (Fig. 2A). We showed excellent efficacy of peruvoside as therapeutics *via* i.p. administration of 0.59 mg/kg peruvoside daily for 7 days from 2 hpi. The efficacy of peruvoside as therapeutics achieved 100% protective effect ($n = 6$, logrank Mantel-Cox test, $^*P = 0.0043$) (Fig. 2A) up to 21 days post lethal infection. This treatment regime also substantially reduced clinical scores based on physical symptoms of body weight, activity, breathing, movement, and dehydration as compared to EV-A71-infected animals treated with DMSO-PBS which developed severe clinical symptoms of inactivity, loss of body weight, and hind limbs paralysis (Fig. 2B).

To examine the impact on viral infection, toxicity, and pathology of peruvoside as therapeutic against our established EV-A71 murine model, 6 dpi hind limb muscle tissues were harvested and blood serum were collected. The hind-limb viral titres were quantified by viral plaque assay showed about 6 log reduction in viral titre with 99.9% efficacy in inhibiting virus for all of peruvoside-treated EV-A71-infected mice ($n = 6$, $P = 0.0001$,

Table 1 50% effective concentration (EC_{50}), 50% cytotoxic concentration (CC_{50}), and selective index (SI) for all tested viruses upon peruvoside treatment.

Virus	Family	Species	EC_{50}	CC_{50}	SI
EV-A71 (HFM41)	Picornaviridae	Enterovirus A	18.63	3118	167.36
CV-A16	Picornaviridae	Enterovirus A	24.52	3118	127.16
CV-A6	Picornaviridae	Enterovirus A	4.79	3118	650.94
Echovirus 7	Picornaviridae	Enterovirus B	1.62	3118	1924.69
CHIKV	Togaviridae	Chikungunya virus	10.14	5563	548.61
ZIKV	Flaviviridae	Zika virus	14.55	234	16.08
DENV2	Flaviviridae	Dengue virus	18.01	234	12.99
SARS-CoV-2	Coronaviridae	Severe acute respiratory Syndrome-related coronavirus	14.09	1734	123.07
MHV	Coronaviridae	Murine coronavirus	20.83	5222	250.69
HSV	Herpesviridae	Herpes simplex virus 1	19.25	3118	161.97
H1N1	Orthomyxoviridae	Human influenza A	51.39	367	7.14
hRSV	Paramyxoviridae	Human respiratory syncytial virus	45.24	4195	92.72

Kruskal−Wallis test) compared to DMSO-PBS-treated EV-A71-infected mice (Fig. 2C). We also assessed *in vivo* toxicity of peruvoside-treated mice by measuring lactate dehydrogenase (LDH) levels in the serum of mice treated with 2, 10 and 50 μmol/L peruvoside. There was no significant difference (one-way ANOVA with post-hoc Dunnett's Multiple Comparison Test) in serum LDH levels between mice administered with DMSO-PBS and 2 μmol/L ($P = 0.50$), 10 μmol/L ($P = 0.81$), 50 μmol/L ($P = 0.93$) (Fig. 2D). Our histopathologic analyses revealed massive loss of villi structures in large intestines and loss of tissue integrity with substantial muscle necrosis in hind limb skeletal muscles of DMSO-PBS treated mice upon virus infection. In contrast, we found that peruvoside-treated EV-A71-infected mice retained organized tissue integrity and revealed no obvious necrosis in small intestine and hind limb skeletal muscles (Fig. 2E). These results demonstrated the *in vivo* potent efficacy of peruvoside against EV-A71 with no observable adverse effects in our murine model.

3.3. *Peruvoside inhibits viral RNA replication*

The encouraging data showing broad-spectrum activity against positive-sense RNA viruses made us to move on to determine the stage(s) of infection targeted by peruvoside in an attempt to unravel the mechanism of their antiviral activity. EV-A71 served as the viral model in our following assays to understand the mechanism of action since peruvoside actively inhibited several enteroviruses tested. We employed our discrete construct[18,19] of

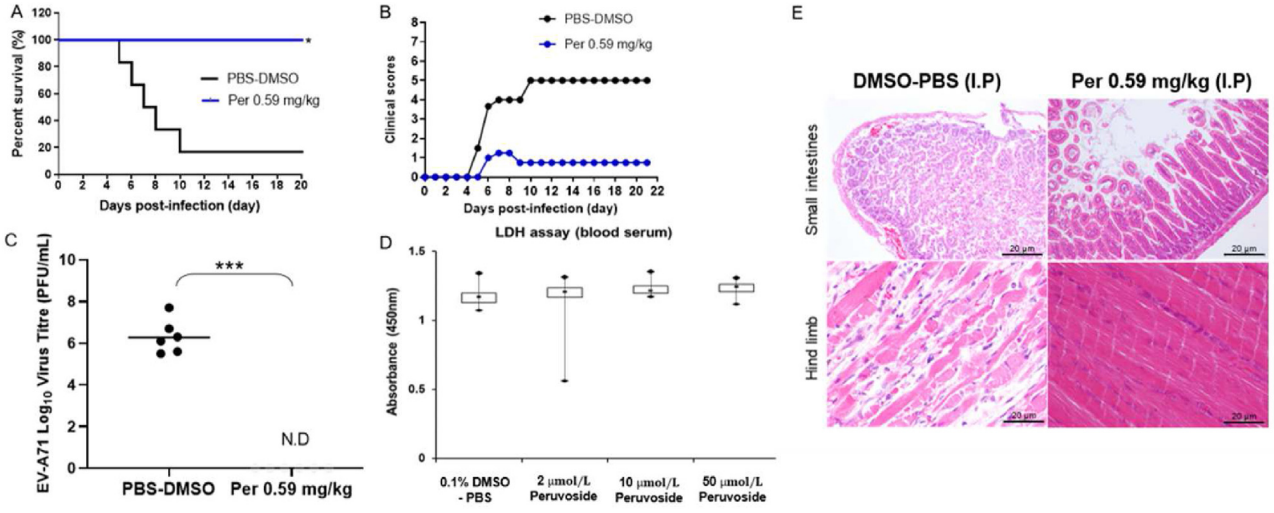

Figure 2 Peruvoside exhibited *in vivo* efficacy against EV-A71 in BALB/c mice. (A) Survival curve of intraperitoneally injected 7-day-old BALB/c mice with 1×10^5 PFU EV-A71 (HFM41) and 0.59 mg/kg peruvoside-treated mice ($n = 6$ mice per group) monitored up to 3-weeks post-infection displayed a significant correlation ($^*P = 0.0043$) by log-rank (Mantel-Cox) test. (B) Clinical scoring evaluated by symptoms of EV-A71 infected mice which includes limb paralysis, ruffled fur, inactivity, rapid breathing and weight loss. (C) Hind-limb viral titration on 6 dpi with EV-A71 and peruvoside-treated EV-A71-infected mice ($n = 6$) displayed a significant reduction of about 6 log ($^*P = 0.0001$) by unpaired *t*-test. (D) LDH assay was performed on serum collected from healthy 7-day-old BALB/c mice administered with 50 μL at indicated concentrations of peruvoside daily for 1 week. Blood was collected at day 8 from start of treatment and assayed for LDH levels. Graph displays box plot with median, upper and lower quartiles. Bars indicate highest and lowest values obtained ($n = 6$ per group). (E) H&E staining of large intestines and hind limb muscle of EV-A71 (HFM41)-infected mice with and without peruvoside treatment. Scale bars represent 20 μm. Error bars indicate standard deviation (SD).

NanoLuc replicon EV-A71 wild-type in which the structural protein coding sequence was replaced by the sequence for NanoLuciferase, and NanoLuc replicon EV-A71 $3D^{def}$ which has a partial C-terminal deletion in the viral RNA-dependent RNA polymerase 3D to represent a viral RNA replication-deficient mutant (Supporting Information Fig. S2A) in order to distinguish the mechanism of peruvoside inhibitory activity on viral replication and/or translation. Using known inhibitors of enteroviral RNA replication or translation (guanidine hydrochloride and cycloheximide, respectively) as controls, we showed that 25, 50, and 100 nmol/L peruvoside treatment resulted in a significant 24.7%, 25% and 31.1% decrease in luminescence, respectively compared to 0.1% DMSO treatment (Fig. S2A). With the replication-deficient $3D^{def}$ mutant replicon we observed a significant 20.7% decrease in luminescence only with 100 nmol/L peruvoside treatment (Fig. S2A), compared 0.1% DMSO treatment. We showed that the mechanism of peruvoside action on EV-A71 replication is *via* inhibition of viral RNA replication, and to a lesser extent *via* viral protein synthesis.

We performed electron microscopy imaging on EV-A71 infected RD cells to visualize the impact of peruvoside treatment on EV-A71-infected RD cells and the appearance of virus-induced morphological changes. As has been reported for several picornaviruses, we observed the generation of DMV (arrows) or viral factories in EV-A71-infected cells that accumulated as infection progressed (Fig. S2B). Our images showed that electron-dense progeny virions (arrowheads) could be observed during late stages of infection (12 hpi onwards) (Fig. S2B). In contrast, EV-A71-infected and peruvoside-treated cells abolished the formation of DMVs at all time-points observed and the organelle structures appeared to be intact, similar to mock-infected and 0.1% DMSO-treated control cells (Fig. S2B). Taken together, our electron microscopy imaging showed that disruption of viral factories (Fig. S2B) was involved in inhibition of EV-A71 viral RNA replication in infected and peruvoside-treated cells.

3.4. *Calcium flux and Src-ERK activation contribute to antiviral effects of peruvoside*

Modulation of intracellular calcium ion (Ca^{2+}) levels *via* influx of extracellular calcium ions or intracellular calcium store release are known mechanisms for plant-derived glycosides[7,22]. To determine if inhibition of the Na^+/K^+ ATPase which actively pumps out sodium ions while bringing in potassium ions that may lead to modulation of Ca^{2+} levels in cells was sufficient for the inhibition of EV-A71 replication, we used chlormadinone acetate (CMA). CMA is an inhibitor of Na^+/K^+ ATPase that does not induce the positive inotropic effects seen with saponin glycosides. We added a range of concentration from 20 to 10,000 nmol/L in EV-A71 infected cells. However, we found that no inhibition of virus infection was observed in EV-A71-infected RD cells (Supporting Information Fig. S3A). Ergo we confirmed that signaling events downstream of the Na^+/K^+ ATPase were essential for EV-A71 replication[23] and not the function of the ATPase itself.

We then assessed cytosolic free Ca^{2+} concentration changes over time with peruvoside-treatment using Fluo-4NW Calcium Assay Kit which detects intracellular free Ca^{2+} in the cytoplasm of stained peruvoside-treated mock-infected and peruvoside-treated EV-A71-infected cells. Basal level of free Ca^{2+} were determined using mock-infected RD cells and capped <5% in mean value. Using one-way ANOVA analysis, we showed that significantly higher percentage of cytosolic free Ca^{2+} levels (>30%) above basal level were observed in peruvoside-treated cells and peruvoside-treated EV-A71-infected cells compared to 0.1% DMSO treated (<10%) (Fig. 3A). In addition, the accompanying increase in free Ca^{2+} levels in peruvoside-treated cells and peruvoside-treated CHIKV-infected cell showed that significantly higher percentage of cytosolic free Ca^{2+} levels (>22%) above basal level were observed (Fig. 3B) determined by basal level of free Ca^{2+} using mock-infected SJCRH30 cells capped <5% in mean value. The accompanying increase in free Ca^{2+} levels in peruvoside-treated RD and SJCHR30 cells, and peruvoside-treated EV-A71- and CHIKV-infected cells, are indicated by the second peak shifts in the flow cytometry histograms towards higher signal strength (Supporting Information Fig. S3B, S4A and Fig. 3).

Cytosolic free calcium levels conceivably were the effector for peruvoside's inhibition of EV-A71 and CHIKV infection. Thus, we subjected peruvoside-treated EV-A71-infected cells to treatment with several calcium channel inhibitors. KB-R9743 and nifedipine, are inhibitors of plasma membrane Ca^{2+} channels, Na^+/Ca^{2+} exchanger and L-type voltage-gated channels respectively. PP2 and neomycin are inhibitors of Src kinase and PLC kinase respectively, were also used to assess if the 'alternative' signaling pathway was also involved in peruvoside's inhibitory activity on EV-A71. We found that all Ca^{2+} channel inhibitors were able to increase EV-A71 titre by $1-\log_{10}$ units in peruvoside-treated cells individually (Fig. S4B). Combination treatments with KB-R9743 + nifedipine and PP2 + neomycin resulted in a significant $2\text{-}\log_{10}$ units ($^{**}P < 0.01$) increase in virus titre in peruvoside-treated infected cells. Finally, triple combination treatment with both Ca^{2+} channel inhibitors and neomycin enhanced the infection, elevating the virus titre higher to greater than $2\text{-}\log_{10}$ units increase compared to peruvoside-treated infected cells (Fig. S3B).

Given the PP2 treatment alone could partially rescue the infection in peruvoside-treated cells, we tested the PLC kinase inhibitor neomycin in a dose-dependent manner. We found that neomycin treatment was able to significantly increase EV-A71 percentage of infection at concentration of 2 mmol/L in peruvoside-treated RD cells (Fig. 3C). Similarly, we tested neomycin treatment in CHIKV infected SJCRH30 cells, which showed about 1.5 log and 2 log increases in viral titre post-treatment of neomycin at 1 and 2 mmol/L, respectively, in peruvoside-treated SJCRH30 cells (Fig. 3D). Following that, PLC activator, m-3M3FBS effect on EV-A71 and CHIKV viral titre were assessed. Our results showed that m-3M3FBS inhibited EV-A71 replication in treated cells in a dose-dependent manner with a significant inhibition at 20 μmol/L ($^{*}P < 0.05$) and 25 μmol/L ($^{**}P < 0.01$) (Fig. 3E). Similarly, m-3M3FBS inhibited CHIKV replication in treated cells with a significant inhibition at 10 μmol/L ($^{*}P < 0.01$) (Fig. 3F). These findings confirmed the sensitivity of peruvoside's antiviral activity through modulation of intracellular free Ca^{2+} levels *via* both 'ionic' and 'alternative' signaling pathways.

We employed siRNA knockdown for different calcium channels that regulate Ca^{2+} release from intracellular Ca^{2+} stores *via* IP_3-signaling (IP_3 receptors, *ITPR1-3*) and Ca^{2+}-induced Ca^{2+} release or CICR, (ryanodine receptors, *RYR*) to divulge peruvoside's mechanism(s). Gene silencing of intracellular calcium channels was confirmed with Fluo-4NW Calcium Assay Kit and showed lower than basal levels of calcium expression in cytoplasm of cells compared to control (NT) (Supporting Information Fig. S5). We showed that silencing of *ITPR3* or *RYR1* resulted in

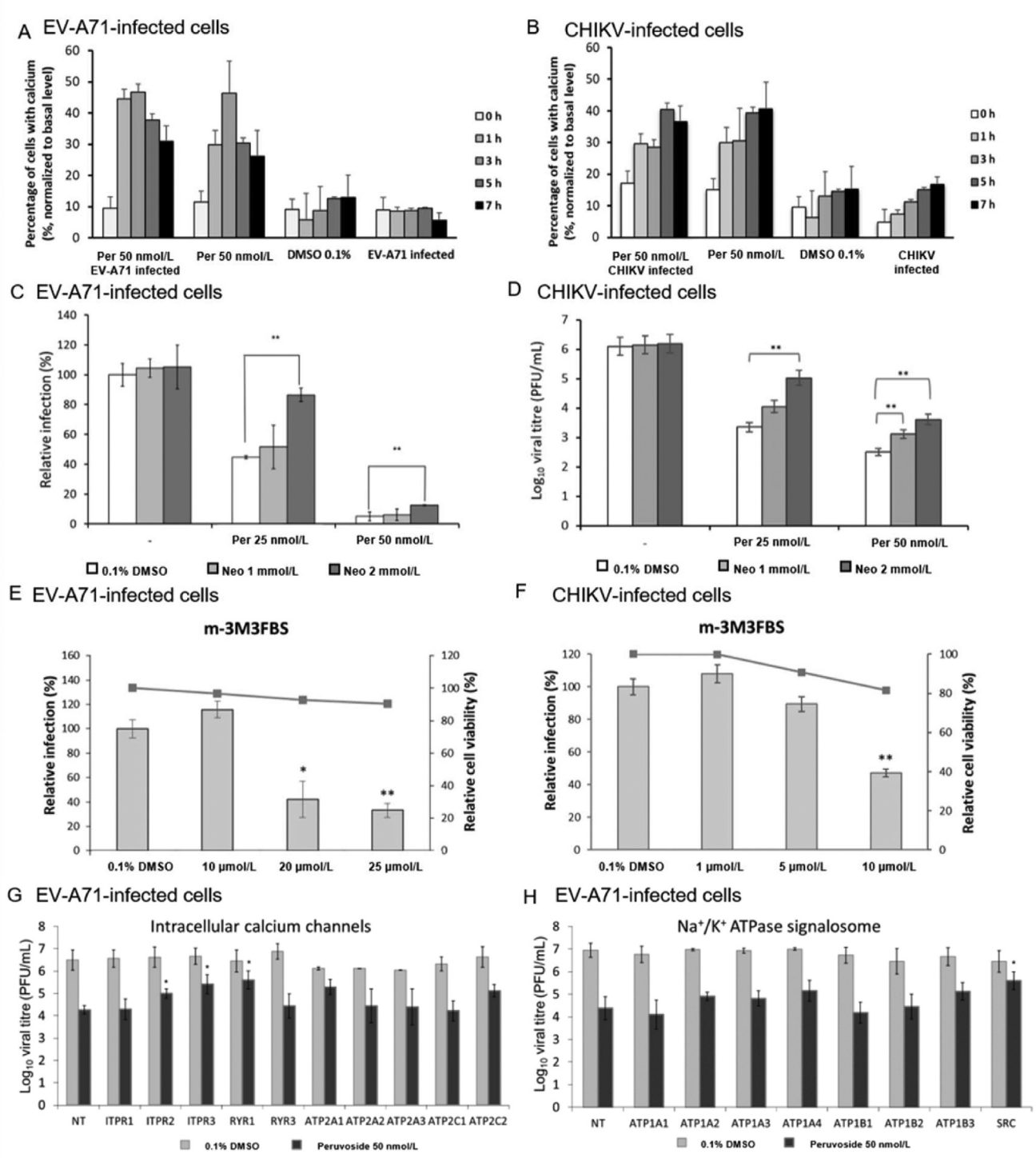

Figure 3 Intracellular calcium signaling is essential for antiviral mechanism of peruvoside. (A) Intracellular Ca^{2+} reserve level upon treatment with peruvoside or 0.1% DMSO, with or without EV-A71 infection, was determined at indicated time-points using flow-cytometry. Data represent the mean value of 3 independent replicates, $n = 3$. (B) Intracellular Ca^{2+} reserve level upon treatment with peruvoside or 0.1% DMSO, with or without CHIKV infection, was determined at indicated time-points using flow-cytometry. Data represent mean value of 3 independent replicates, $n = 3$. (C) EV-A71-infected RD cells were treated with PLC-inhibitor, neomycin, at indicated concentrations and relative infection percentage was determined at 12 hpi with indirect immunofluorescence staining for viral antigen VP2. (D) CHIKV-infected SJCRH30 cells were treated with PLC-inhibitor, neomycin, at indicated concentrations and viral titre infection percentage was determined at 24 hpi with plaque assay. (E) EV-A71-infected RD cells were treated with PLC-activator, m-3M3FBS, at indicated concentrations and relative infection percentage was determined at 12 hpi with indirect immunofluorescence staining for viral antigen VP2. (F) CHIKV-infected SJCRH30 cells were treated with PLC-activator, m-3M3FBS, at indicated concentrations and viral titre infection percentage was determined at 24 hpi with plaque assay. (G) Knockdown of selected

the strongest rescue of EV-A71 viral titre (>1−$\log_{10}$ units increase) (Fig. 3G) and there was an increased basal level of Ca^{2+} shown by peak shifts in the flow cytometry histograms (Fig. S5) in peruvoside-treated cells. Additionally, we also investigated the impact of silencing Ca^{2+} reuptake channels on the antiviral activity of peruvoside by silencing *ATP2C1-2* that encode for calcium reuptake channels on the Golgi secretory pathway calcium ATPase, and *ATP2A1-3* encoding for ER channels, sarco/endoplasmic reticulum calcium ATPases. Silencing of *ATP2C1-2*, and *ATP2A1-3* showed that only *ATP2A1* resulted in at least 1−$\log_{10}$ units increase in EV-A71 titre (Fig. 3G). siRNA knockdown of these calcium channels was confirmed using Fluor-4NW calcium assay evincing lower than basal levels of calcium concentration compared to control (NT) *via* histogram peak shifts (Fig. S5).

Further, we performed silencing of individual isoforms of the α- and β-subunits of Na^+/K^+ ATPase, upstream of intracellular Ca^{2+} release. Our results showed that it did not significantly impact peruvoside inhibition of EV-A71 (Fig. 3H). However, knockdown of Src expression resulted in an almost complete recovery of EV-A71 replication with a viral titre just 1−$\log_{10}$ units lower in the presence of peruvoside compared to untreated cells (Fig. 3H). Thus far these results support that intracellular calcium flux is an essential mechanism of peruvoside's antiviral activity and the calcium flux is mediated *via* both the 'ionic' pathway of extracellular calcium influx and the 'alternative' pathway of PLC/IP_3 signaling. The release of calcium from intracellular stores is one of the triggering events for ER stress and the unfolded protein response[24], while premature activation of these processes can halt protein synthesis, initiate apoptosis and inhibit virus replication[25]. Although our results in Fig. S2A show limited inhibition in viral RNA translation post peruvoside treatment, we nonetheless investigated if ER stress plays a role in the inhibition of EV-A71. ER stress response was ruled out using three key markers of ER stress which showed no alternative splicing of X-box binding protein 1 (*XBP1*) mRNA, no cleavage of phospho-ATF6 and no elevated phospho-PERK levels in peruvoside-treated cells (Supporting Information Fig. S6A−S6C). In addition, we performed indirect immunofluorescence staining of Calnexin, the calcium binding ER chaperone has been shown to be a good predictor of cell sensitivity to ER stress-mediated cell death[26]. Our staining did not reveal any overt morphological change to the ER with peruvoside treatment indicating no signs of ER stress (Fig. S6D).

3.5. *Peruvoside causes perinuclear vesiculation of Golgi and GFB1 phosphorylation*

The major intracellular calcium stores, ER and Golgi, are also organelles necessary for enteroviral replication[27,28]. Moreover, enterovirus viral non-structural protein 3A has been shown to associate with host protein, GBF1 on the cytoplasm-facing intracellular membranes to recruit components of the retrograde transport coat protein complex (COPI), and other essential factors for replication such as phosphatidylinositol-4-kinase IIIβ (PI4K3β) in aid of viral replication[29,30]. Hence, these studies prompt an assessment of changes in the Golgi upon peruvoside treatment. Immunofluorescence staining of Golgi marker (GM130) and granularity of Golgi were measured using CellProfiler (version 2.2.0)[20] which revealed Golgi vesiculation and significantly enhanced granularity following treatment with peruvoside, brefeldin A (BFA) and m-3M3FBS (Fig. 4A). BFA was included as a positive control as it is a well-studied inhibitor of enteroviruses, DENV and CHIKV known to cause Golgi dispersal and redistribution into the ER network[31−33]. We observed that Golgi fragmentation triggered by BFA was dispersed in a cell-wide manner with diffused GM130 signals in contrast to peruvoside-induced Golgi vesiculation which showed a distinct perinuclear pattern. Convincingly, the non-positively inotropic CMA did not show Golgi vesiculation (Fig. 4A) and no significant increase in granularity (Fig. 4A) whereas neomycin resulted in a significant decrease in Golgi granularity in peruvoside-treated cells (Fig. 4A). Roscovitine, similar to neomycin, an inhibitor of CDK1 reported to phosphorylate GBF1[34] was effective in reducing Golgi granularity in peruvoside-treated cells (Fig. 4A), suggesting the involvement of GBF1 in peruvoside-induced Golgi vesiculation. Roscovitine was assessed in EV-A71- and CHIKV-infected cells treated with peruvoside. Our results show that roscovitine at 2 and 5 μmol/L significantly ($^*P < 0.05$) and partially increase the fraction of peruvoside-treated EVA71-infected cells by approximately 10%−15% when compared to 0.1% DMSO-treated cells (Fig. 4B) and in peruvoside-treated CHIKV-infected cells by approximately 0.25 log−0.5 log when compared to 0.1% DMSO-treated cells (Fig. 4C). These results indicate involvement of CDK1 in GBF phosphorylation following peruvoside treatment.

Golgi undergoes extensive vesiculation during mitosis in a regulated process involving the phosphorylation of GBF1 at Threonine 1337[34,35]. Thus, we used phospho-GBF1 targeted antibody against Threonine 1337 in our western blotting analysis. We confirmed elevated level of GBF1 phosphorylated at Threonine 1337 (T1337) in cells treated with peruvoside and m-3M3FBS compared to 0.1% DMSO-treated RD cells (Fig. 4D). M-3M3FBS, neomycin and roscovitine were able to partially neutralize the effect of peruvoside by reducing the amount of phospho-GBF1 (Fig. 4D), whereas BFA did not result in higher phospho-GBF1 levels even though it could also trigger Golgi vesiculation (Fig. 4D), implying a different mechanism from peruvoside. Treatment with CMA which did not inhibit EV-A71 replication (Fig. S3A) also did not increase the level of phospho-GBF1 (Fig. 4D). Similar conditions were observed in peruvoside treated SJCRH30 cells with M-3M3FBS, neomycin and roscovitine being able to reduce the amount of phospho-GBF1, whereas BFA did not result in increases of phospho-GBF1 (Fig. 4E). The authenticity of the phospho-GBF1 bands were validated by treatment with alkaline phosphatase which removed phosphorylated GBF1 bands. All phospho-GBF1 bands in peruvoside-treated or BFA-treated or EV-A71-infected cell

intracellular calcium channel proteins and (H) Knockdown of selected components of the Na^+/K^+ ATPase signalosome using siRNA was performed for 3 days on RD cells then infected with EV-A71 and treated with 50 nmol/L peruvoside or 0.1% DMSO. All bar graphs presented were an average of 3 experiments (2 technical replicates/experiment) and statistical analysis was performed by unpaired, two-tailed Student's *t*-test against 0.1% DMSO, error bars reflect standard deviation (SD). $^*P < 0.05$, $^{**}P < 0.01$, $n = 3$. Cell viability assay and infection assay was performed with RD cells treated for 12 h and SJCRH30 cells treated for 24 h, and relative cell viability was expressed as a percentage compared to 0.1% DMSO-treated cells.

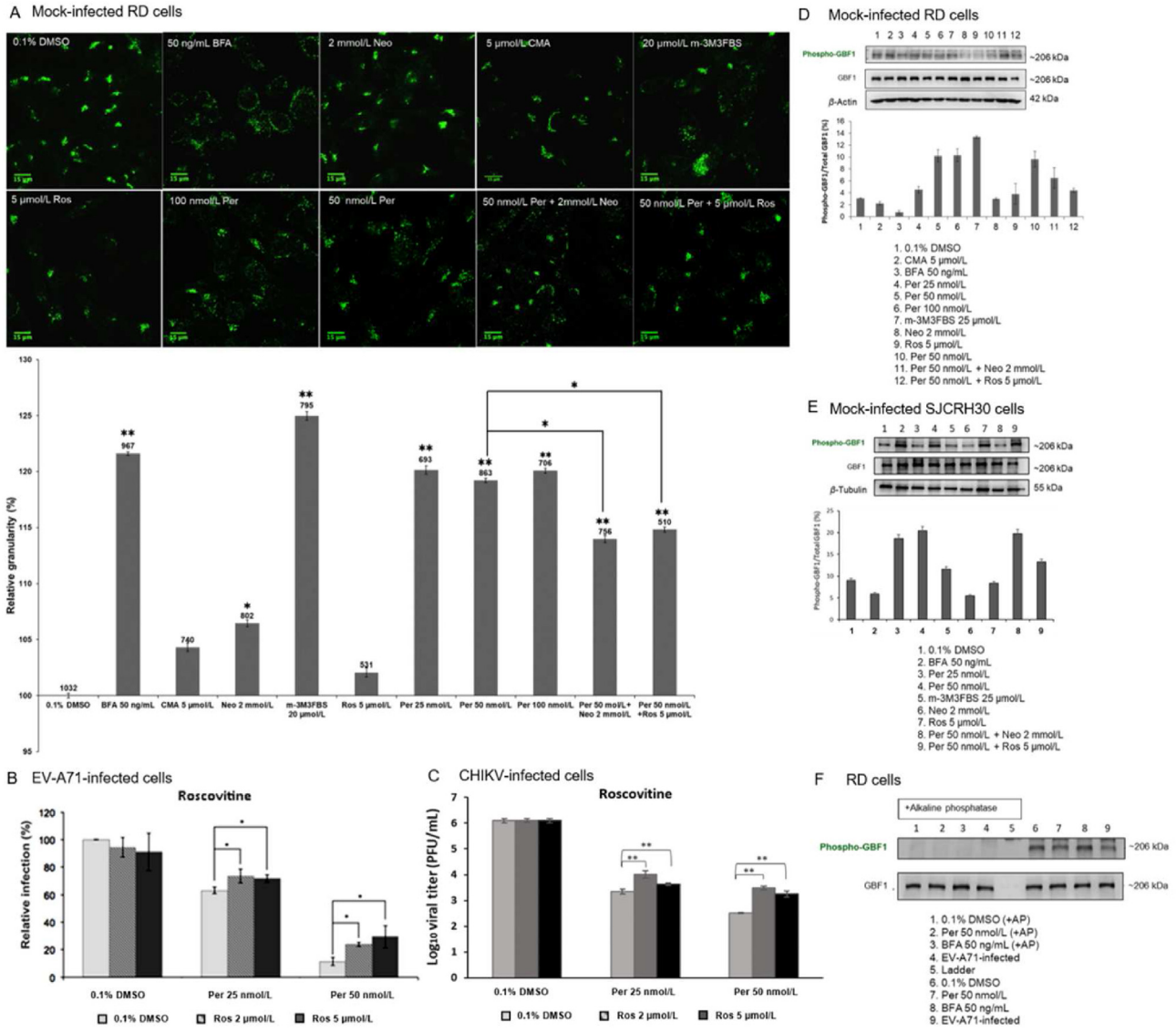

Figure 4 Peruvoside treatment induced Golgi vesiculation and GBF1 phosphorylation. (A) Immunostaining of Golgi marker GM130 was performed for various compounds on RD cells and were treated for 12 h. Vesiculation of the Golgi was quantified using CellProfiler. Numbers atop bars indicate total number of cells analyzed from 3 experiments. Asterisks above bars are indicative of P values from unpaired, two-tailed Student's t-test against 0.1% DMSO. $*P < 0.05$, $**P < 0.01$; $n = 3$. Error bars indicate standard deviation (SD). (B) Immunofluorescence was performed at 12 hpi with the addition of roscovitine (CDK1 inhibitor) to peruvoside treated EV-A71 strain H infected cells. Percentage of infected cells was derived from the number of cells expressing viral specific marker VP2 and total nuclei count. (C) Viral titration was performed at 24 hpi with the addition of roscovitine (CDK1 inhibitor) to peruvoside treated CHIKV infected cells. Statistical analysis by from two-way analyses of variance (ANOVAs) was performed against 0.1% DMSO. $*P < 0.05$; $n = 3$. (D) RD cells were treated with 0.1% DMSO (negative control), chlormadinone acetate (CMA), brefeldin A (BFA), peruvoside (Per) at different concentrations, m-3M3FBS, neomycin (Neo) and roscovitine (Ros) or in combinations for 12 h and total cell lysates were harvested for Western blotting. (E) SJCRH30 cells were treated with 0.1% DMSO (negative control), BFA, Per at different concentrations, m-3M3FBS, Neo and Ros or in combinations for 24 h and total cell lysates were harvested for Western blotting. All RD cell and SJCRH30 membranes were probed with antibodies against GBF1, phospho-GBF1 and β-actin and β-tubulin (loading control), respectively. Quantification of band intensities was performed with Image Studio (LI-COR) and the abundance of phospho-GBF1 was expressed as a percentage of total GBF1 for each treatment condition. Results presented are an average of three experiments and error bars reflect SD, $n = 3$. (F) Western blot was performed with total cell lysates of RD cells treated with 0.1% DMSO, Per, BFA or infected with EV-A71 and a duplicate set of lysates was treated with alkaline phosphatase (AP) for 30 min at 37 °C. The blots were probed with a specific antibody against phosphorylated GBF1 at T1337 and total GBF1 to confirm the specificity of the phospho-GBF1 band detected.

lysate were diminished post alkaline phosphatase treatment as opposed to no treatment (Fig. 4F).

Peruvoside exhibited inhibitory activity on viruses from multiple families, thus alluding to an analogous mechanism of Golgi vesiculation and disruption of viral replication. Hence, we performed immunofluorescence for Golgi (GM130) and viral dsRNA (dsRNA is produced as a replicative intermediate during RNA virus replication) in peruvoside-treated and 0.1% DMSO-treated

and viral infected cells. Our results revealed Golgi stacks vesiculation within a perinuclear distribution pattern upon treatment with peruvoside in cells infected with EV-A71 (Fig. 5A), CHIKV (Fig. 5B), ZIKV (Fig. 5C), DENV2 (Fig. 5D) and MHV (Fig. 5E). We also found that Golgi vesiculation was associated with the absence of viral dsRNA in cells infected with EV-A71 and CHIKV observed at 12 (Fig. 5A) and 24 hpi (Fig. 5B), respectively. We also found considerably lower detection of viral dsRNA in Huh7 cells infected by ZIKA and DENV2 at 48 h (Fig. 5C and D) and less viral dsRNA in H2.35 cells infected by MHV at 24 h (Fig. 5E) when compared to control cells treated with 0.1% DMSO. These data were consistent with the viral titre reduction in peruvoside-treated cells.

Since roscovitine diminished the effect of peruvoside on Golgi vesiculation (Fig. 4A), it could imply an essential involvement of GBF1 in peruvoside-induced Golgi vesiculation. Our inferences are based on various reports implicating the association of EV-A71, CHIKV, ZIKA, DENV2 and SARS-CoV-2 infection and replication[29,30,33,36,37] with GBF1 as well as its role in the biogenesis of Golgi structures. Hence, we performed immunofluorescence staining of Golgi and GBF1 in peruvoside-treated and 0.1% DMSO-treated cell lines used for viral infection in this study. Extensive colocalization of GBF1 and GM130 (Golgi marker) in the perinuclear region of RD cells at 12 h post-treatment (hpt) (Fig. 6A), in SJCRH30 cells at 24 hpt (Fig. 6B), in Huh7 cells at 48 hpt (Fig. 6C) and in H2.35 cells at 24 hpt (Fig. 6D) were observed. Taken together, our results validate the GBF1 involvement in Golgi vesiculation in peruvoside-treated cells.

To understand GBF1 involvement in peruvoside-treated cells and its role in peruvoside-treated viral-infected cells, we performed Western blotting on GBF1, GBF1 phosphorylation and viral proteins. Initial Western blot densitometry analysis of mock-infected cells showed increasingly higher levels of phosphorylated GBF1 in peruvoside-treated cells compared to 0.1% DMSO-treated cells in RD cells (Fig. 6E), SJCRH30 cells (Fig. 6F) and Huh7 (Fig. 6G) cells. Western blot analysis and bar graph plot in virus infected cells corroborated increasingly higher levels of phosphorylated GBF1 in peruvoside-treated cells than 0.1% DMSO-treated control cells for EV-A71-infected RD cells (Fig. 7A). Similarly, CHIKV-infected SJCRH30 cells showed increasing levels of phosphorylated GFB1 in a time-dependent manner which was not evident in 0.1% DMSO-treated viral-infected cells (Fig. 7B). ZIKA (Fig. 7C) and DENV2-infected (Fig. 7D) Huh7 cells also showed gradual increase in phosphorylated GBF1 levels in cells as opposed to 0.1% DMSO-treated viral-infected cells. Expectedly, EV-A71 viral protein VP0 was not detected at all time points in peruvoside-treated cells as compared to 0.1% DMSO-treated cells which showed viral protein at 6 h post-infection (Fig. 7A and E). In CHIKV-infected SJCRH30 cells, capsid protein expression was detectable at all time points but observed to be consistently lower in peruvoside-treated cells (Fig. 7B and F). ZIKV (Fig. 7C and G) and DENV2 (Fig. 7D and H) envelope protein expression was consistently lower in peruvoside-treated cells and was only detectable at 36 h post-infection compared to 0.1% DMSO-treated cells which expressed envelop protein at 24 h post-infection. These findings confirm that GBF1 phosphorylation associates with peruvoside's mechanism of viral RNA replication inhibition for the tested viruses.

3.6. GBF1 is phosphorylated via CDK1 during peruvoside-treatment

Ouabain, a compound from the same class as peruvoside has been shown to activate the extracellular signal-regulated kinases (ERK) in a Src-dependent manner[8]. The calcium flux and Src kinase signaling cascades[38,39] described in Fig. 3 may possibly trigger

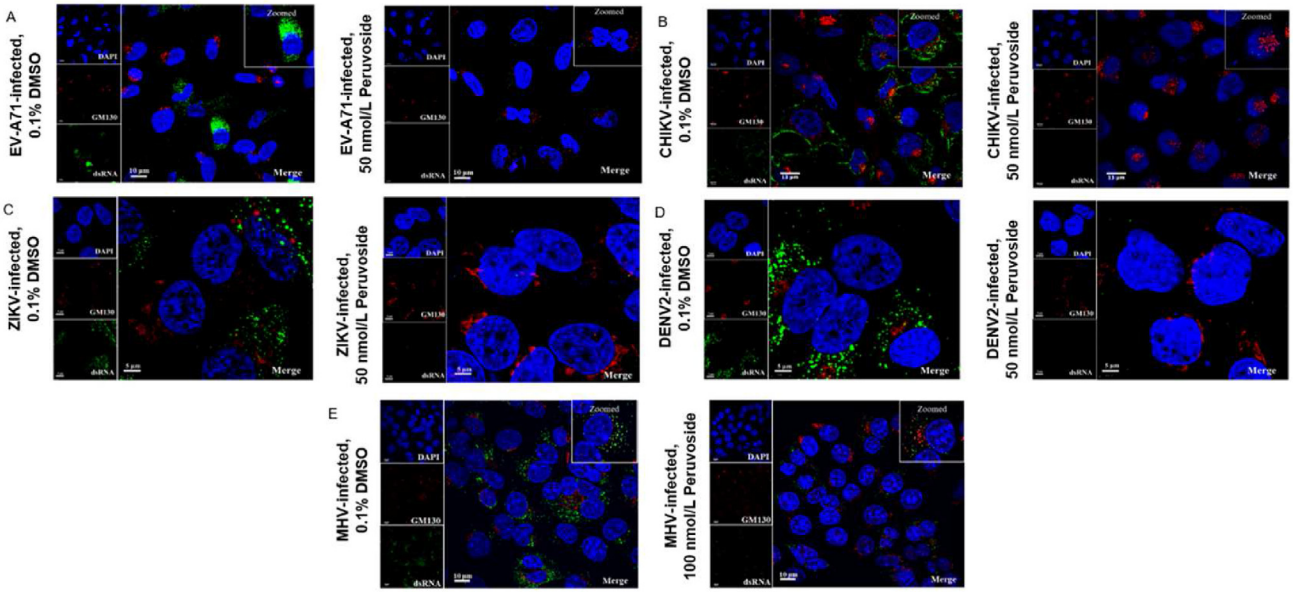

Figure 5 Peruvoside treatment induced Golgi vesiculation and reduced viral RNA replication. (A) EV-A71-infected RD cells were treated with the peruvoside or 0.1% DMSO for 12 h were immunofluorescence stained. (B) CHIKV-infected SJCRH30 cells were fixed at 24 hpi and immunofluorescence stained (C) ZIKV-infected and (D) DENV2-infected Huh7 cells with peruvoside or 0.1% DMSO treatment were immunofluorescence stained at 48 hpi. All cells were fixed, and immunofluorescence stained for Golgi-specific marker, GM130 (red) and dsRNA (green). Nuclei were counterstained with DAPI (blue).

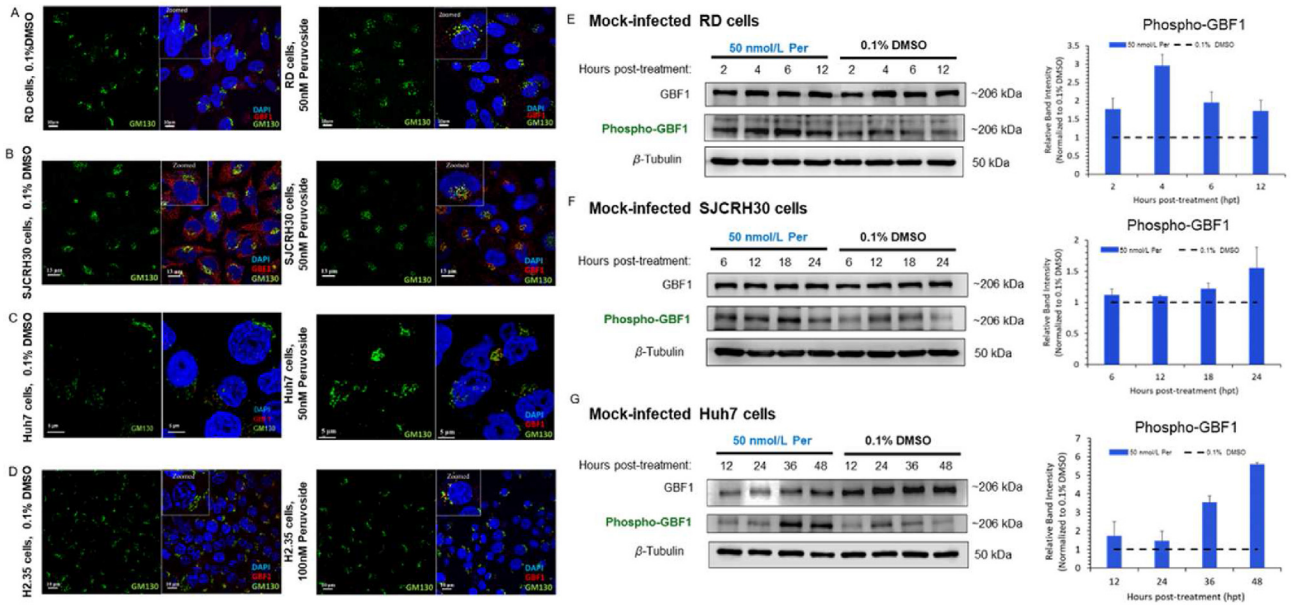

Figure 6 GBF1 was phosphorylated upon peruvoside treatment and colocalized with GM130 in peruvoside treated cells. (A) Western blotting was performed on total cell lysates of RD cells, (B) SJCRH30 cells and (C) Huh7 cells treated with 50 nmol/L peruvoside or 0.1% DMSO and probed with antibodies against GBF1 and phospho-GBF1. Quantification of band intensities was performed with Image Studio (LI-COR). All bar graphs show phosphorylated GBF1 expression normalized with 0.1% DMSO treated cells. β-Tubulin was included as a loading control. Densitometry results presented were an average from 3 experiments normalized against 0.1% DMSO-treated mock samples and error bars reflect SD ($n = 3$). All bar graphs show relative band intensities normalized with 0.1% DMSO-treated infected cells. (D) RD cells were treated with the indicated compounds for 12 h. (E) SJCRH30 cells were treated with the indicated compounds for 24 h. (F) Huh7 cells were treated with the indicated compounds for 48 h. (G) H2.35 cells were treated with the indicated compounds for 24 h. Colocalization of GBF1 and GM130 were determined in merged image (yellow) for all cells. Cells were fixed and immuno-stained for Golgi-specific marker, GM130 (green) and GBF1 (red). Nuclei were counterstained with DAPI (blue).

pathways known to regulate CDK1 and GBF1 activities, which led us to determine the ERK1/2 phosphorylation status in peruvoside-treated cells. Indeed, our Western blotting analysis showed an increase in phosphorylated ERK1/2 upon peruvoside treatment in comparison to 0.1% DMSO-treated RD cells and EV-A71-infected RD cells (Fig. 8A), as well as in 0.1% DMSO-treated SJCRH30 cells and CHIKV-infected SJCRH30 cells (Fig. 8B). Following that, specific inhibitors of CaMK1, KN93 and, specific inhibitor of ERK1/2, FR180204 were then used to disrupt peruvoside's antiviral signaling *via* these pathways. We found that specific inhibitor of CaMK1 with 50 nmol/L peruvoside-treated cells showed significant recovery of EV-A71 infection in response to increasing doses of KN93 concentration from 5, 7.5 to 10 μmol/L in 50 nmol/L peruvoside-treated RD cells (Fig. 8C) and showed significant recovery of CHIKV infection in response to increasing dose from 5 μmol/L in 50 nmol/L peruvoside-treated SJCRH30 cells, and 7.5 to 10 μmol/L in both 25 and 50 nmol/L peruvoside-treated SJCRH30 cells (Fig. 8D). ERK1/2 inhibitor also showed significant recovery of EV-A71 infection with increasing doses of FR180204 concentration from 5, 7.5 to 10 μmol/L in 50 nmol/L peruvoside-treated RD cells (Fig. 8E). Similarly, a significant recovery of CHIKV infection with increasing doses of FR180204 concentration from 5, 7.5 to 10 μmol/L in 50 nmol/L peruvoside-treated SJCRH30 cells were observed (Fig. 8F). These results demonstrate the involvement of ERK1/2 pathway and reconcile the observations of GBF1 phosphorylation with calcium flux induced by peruvoside which worked to inhibit the replication of EV-A71.

Finally, we were able to significantly ($^{**}P < 0.01$) rescue EV-A71 infection from peruvoside treatment at 25 and 50 nmol/L with the overexpression of wild type GBF1 (WT) or GBF1 with a non-phosphorylable alanine substitution mutation at T1337 (T1337A) (Fig. 8G). We included cells expressing only V5-tag (V5) and non-transfected RD cells (RD) as negative controls. The overexpression of phosphomimetic mutant of GBF1 carrying a glutamic acid substitution (T1337E) did not result in significant improvement in EV-A71 infection rates for all peruvoside concentration tested, similar to negative controls (Fig. 8G). Taken together, we have dissected and mapped out the complex detail drug target of peruvoside as a broad-spectrum antiviral against positive-sense RNA virus which is mediated by GBF1 phosphorylation *via* CDK1 activation of ERK1/2 pathway that triggers extensive Golgi vesiculation hence damping the formation and function of viral replication complexes.

4. Discussion

All positive-sense RNA viruses modify existing intracellular membranes and hijack host membrane structures to generate membranous replication organelles. These organelles are believed to provide a protected and conducive environment for virus replication, concentrating essential host and viral factors while subverting innate immune response[40,41]. The generation of these structures during virus replication is highly regulated and coordinated with viral protein synthesis and RNA replication[42], which is the very reason why many antivirals are designed to target viral

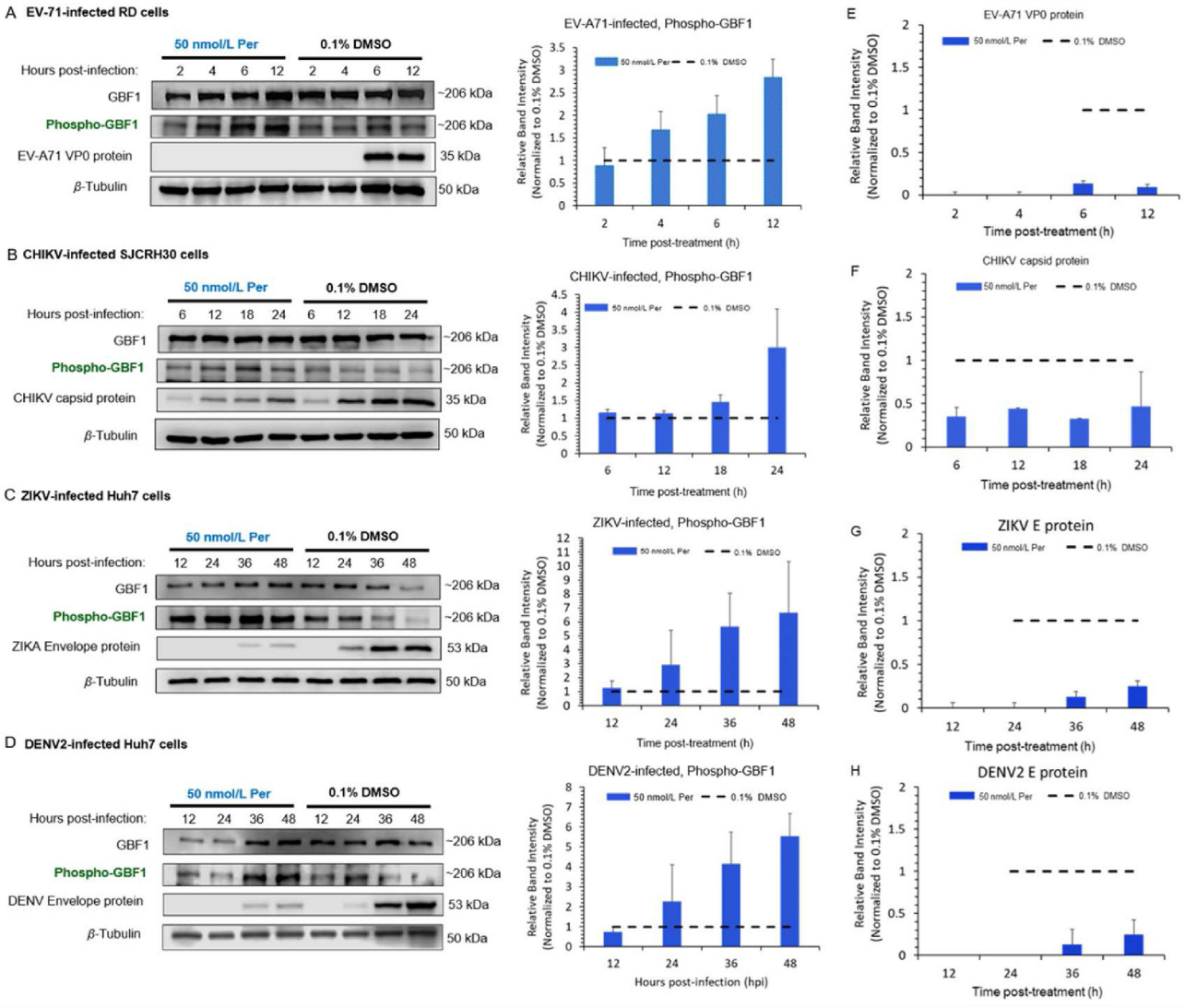

Figure 7 GBF1 was phosphorylated and viral proteins reduced in virus-infected peruvoside-treated cells. (A) Western blotting was performed on total cell lysates of EV-A71-infected RD cells treated with different compounds and probed with antibodies against GBF1 and phospho-GBF1. (B) Western blotting was performed on total cell lysates of CHIKV-infected SJCRH30 cells. (C) Western blotting was performed on total cell lysates of ZIKV-infected and (D) DENV2-infected Huh7 cells. Quantification of band intensities was performed with Image Studio (LI-COR) for (E) EV-A71 VP0, (F) CHIKV capsid, (G) ZIKV E protein and (H) DENV2 E protein with Western blots presented in A−D. All bar graphs show phospho-GBF1 expression normalized to 0.1% DMSO treated cells. Tubulin was included as a loading control. Bar graph presented was an average from three experiments normalized against 0.1% DMSO-treated mock samples and error bars reflect SD; $n = 3$.

genome and viral protein synthesis. In our study using peruvoside, we discovered that saponin glycosides can trigger extensive Golgi vesiculation linked to PLC-mediated Ca^{2+} signaling and GBF1 phosphorylation which led to inhibition of viral replication. Using electron microscopy, Whetsell and Bunge first observed loss of Golgi stacks and the appearance of vacuoles in ouabain-treated neurons[43]. With peruvoside, we confirmed the Golgi-origin of these vacuoles and uncovered a link to the 'alternative' signaling mode of action for peruvoside.

Based on the well-characterized effects of certain saponin glycosides on intracellular calcium stores, we found an essential role for calcium flux in peruvoside's mechanism of inhibiting viral replication. Intracellular calcium flux is a highly complex signaling cascade that can trigger a multitude of cell-wide changes where we show intracellular calcium influx in cytoplasm with peruvoside treatment in cells (Fig. 3). Previous study on ouabain has been shown to activate ERK in a Src-dependent manner[8] and intracellular calcium flux will inevitably activate calcium/calmodulin-dependent kinases, which are involved in growth-related pathways such as MAPK/ERK activation. In this study with peruvoside, we proved that inhibition of Src significantly limited peruvoside antiviral activity and increased viral titre (Fig. 3) in a similar pathway. Specifically, CaMK1 has been shown to activate ERK in response to calcium signals[44] and we showed that inhibition of CaMK1 and ERK 1/2 limited peruvoside antiviral activity by significantly recovering viral infection (Fig. 5). Our study preclosed a new phosphorylatable pathways which includes CDK1 involvement in the signaling cascade using

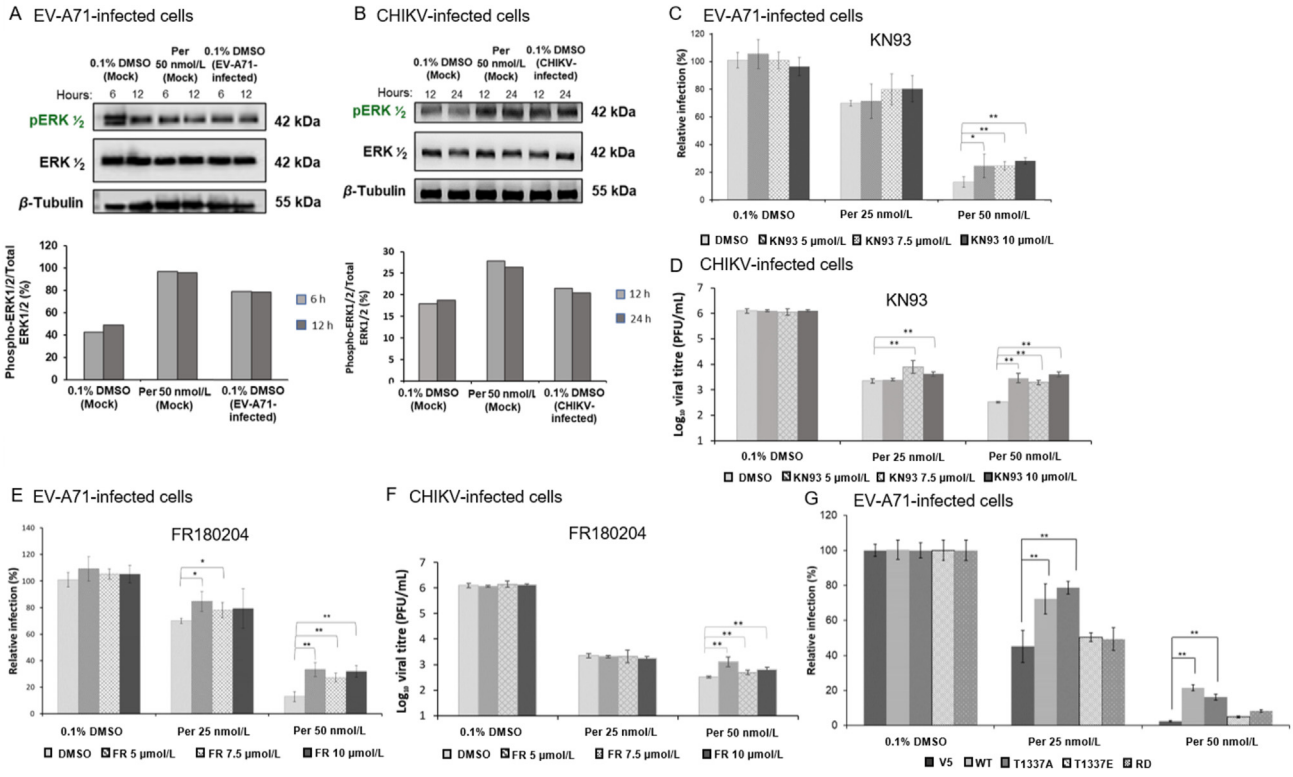

Figure 8 CDK1 mediated GBF1 phosphorylation *via* ERK1/2 pathway. Total cell lysates from indicated time-points and treatment conditions were harvested for Western blotting and probed for pERK1/2 levels relative to total ERK1/2 and β-tubulin in (A) RD cells and (B)SJCRH30 cells. (C) KN93 (CaMKI inhibitor) was added to peruvoside treated EV-A71 strain H infected cells and fixed at 12 hpi for indirect immunofluorescence assay staining for viral antigen VP2. Relative infection was derived from number of cells expressing viral specific marker VP2 and total nuclei count. (D) KN93 (CaMKI inhibitor) was added to peruvoside treated CHIKV-infected cells and viral titration were performed at 24 hpi *via* plaque assay. (E) FR180204 (ERK1/2 inhibitor) was added to peruvoside treated EV-A71 strain H infected cells and fixed at 12 hpi for indirect immunofluorescence assay staining for viral antigen VP2. Relative infection was derived from number of cells expressing viral specific marker VP2 and total nuclei count. (F) FR180204 (ERK1/2 inhibitor) was added to peruvoside treated CHIKV-infected cells and viral titration were performed at 24 hpi *via* plaque assay. (G) Immunofluorescence was performed to determine extent of inhibition of EV-A71 strain H infection by peruvoside in RD cells stably expressing GBF1 (wildtype, WT), non-phosphorylatable mutant (T1337A) or phosphomimetic mutant (T1337E). Infection rates were normalized against respective cell lines treated with 0.1% DMSO. Statistical analysis by unpaired, two-tailed Student's *t*-test was performed for each mutation against WT at each dose of peruvoside. All other statistical analysis by unpaired, two-tailed Student's *t*-test was performed against 0.1% DMSO-treated cells at each dose of peruvoside. $*P < 0.05$ and $**P < 0.01$; $n = 3$. Data presented show the average of three independent experiments (two technical replicates/experiment) and error bars reflect SD.

roscovitine, a known inhibitor of CDK1 which showed no Golgi vesiculation and reversal in relative infection with peruvoside treatment (Fig. 4). Overall, we module that the activation of calcium flux and Src and PLC kinase could trigger this pioneer pathway known to regulate CDK1 and in-turn GBF1 activities with peruvoside treatment.

We showed that peruvoside inhibits RNA viruses from four families of Picornaviridae, Togaviridae, Flaviviridae and Coronaviridae, and one DNA virus, HSV1. Although DNA viruses adopt a different replicative mechanism from RNA viruses, the Golgi apparatus is a common component in its replication cycles[45]. The Golgi and ER are important intracellular stores that sequester free calcium from the cytosol and can generate cell-wide or localized spikes in calcium levels in response to the appropriate signals[46]. Viral proteins, such as enterovirus 2B and rotavirus NSP4, can act as porins to trigger release of calcium from Golgi and ER during late viral replication cycle[47–49]. These seemingly paradoxical antiviral and proviral effects of the same cellular event of calcium flux, can likely be explained by the importance for timely and regulated coordination of cellular changes during virus replication. The premature activation of cellular pathways may deprive viral factors of crucial host factors needed for replication. Our study showed that peruvoside modulate calcium flux in cytoplasm of cells and it is essential for its antiviral activity (Fig. 3). Moreover, we showed that peruvoside also triggered Golgi vesiculation (Figs. 4 and 5) and GBF1 phosphorylation (Fig. 7). The Golgi apparatus is known to be essential for cell survival and division, while it is also known to disassemble and vesiculate, which then reassemble upon cell division completion[50]. Hence, given that Golgi apparatus vesiculates and reassembles in host cells, the cytotoxicity issue can be overcome with the concentration of peruvoside used as an antiviral. Further, in all our experiments with peruvoside treatment (peruvoside <100 nmol/L) we did not notice any adverse effect of cellular death (all experiments were below EC_{50} values). Moreover, our murine model treatment of 0.59 mg/kg for 1-week post-infection did not show any adverse effect in LDH assay (Fig. 2D) indicating no cytotoxicity for the dosage used. We are assertive that

peruvoside's inhibitory mechanism is unlike others as it triggers downstream signaling involving CDK1 activation and GFB1 phosphorylation. It is likely that Golgi disruption on its own is not antiviral but rather the disruption of access to crucial factors needed for viral replication, specifically GBF1 in the case of peruvoside.

GBF1 is a guanine nucleotide exchange factor that regulates COPI recruitment through activation of ADP-ribosylation factor 1 at the ER-Golgi intermediate compartment. It is a large (~206 kDa) multidomain protein that plays multiple roles and has a myriad of interaction partners. Studies in mitotic cells found that GBF1 phosphorylation results in Golgi vesiculation, membrane dissociation, reduced ADP-ribosylation factor 1 activation and other effects beyond COPI recruitment in MHV, CHIKV, DENV2, ZIKV and Influenza virus infection[31,33,35,51–53]. This study also showed that peruvoside treatment caused GBF1 phosphorylation resulting in Golgi vesiculation for different types cells infected with EV-A71, CHIKV, ZIKV, DENV2 and MHV (Fig. 5) as well as reduced viral dsRNA that translated to reduction of viral replication in cells. As known, viruses use GFB1 in the form of non-phosphorylated for regulation of COPI recruitment for formation of viral factories or transport of proteins from ER to Golgi for maturation of proteins[1,28,54]. Hence, phosphorylation of GBF1 may desperately deprive viruses of its function as a COPI recruitment and limit its function on transport of viral proteins form ER to Golgi.

We have shown that the reversal of peruvoside's antiviral effects by various pathway-interfering inhibitors was associated with a reduction in both phospho-GBF1 levels and Golgi vesiculation. Specifically, we showed that GBF1 is colocalized with GM130 (a known Golgi marker) only in peruvoside treated cells as opposed to DMSO treated cells (Fig. 6) to vindicate GBF1 as a key component in causing Golgi vesiculation. To further determine CDK1 phosphorylatable site in GFB1, we showed that the overexpression of wild-type GBF1 and a non-phosphorylatable mutant (T1337A) was able to rescue EV-A71 replication inhibited by peruvoside (Fig. 8). Hence, we discovered that not only AMPK[35], also CDK1 signaling of phosphorylated GBF1 at the site of T1337.

5. Conclusions

Taken together, the results from this study highlight the importance of GBF1 in viral replication. GBF1 plays a role for many viruses from remodeling the intracellular membranes to forming viral replication factories to the recruitment of important lipid-decorating enzymes (such as phosphatidylinositol-4-kinase β or PI4KB), host environment modification[55] and viral assembly/maturation processes[56]. We have shown that GBF1 functions could be made inaccessible to viral factors by inactivation of its phosphorylation triggered by saponin glycosides like peruvoside and the after effect of vesiculation of Golgi may impair viral replication or maturation of viral protein. Our study demonstrated the pleiotropic cellular effects of saponin glycosides from intracellular calcium signaling to modulation of growth-related pathways that led to the GBF1 phosphorylation and Golgi vesiculation, a crucial host factor in viral replication. By targeting host factors/processes shared by many viruses, peruvoside exhibited inhibitory activity on a broad array of RNA viruses. Traditional antiviral development has focused largely on direct-acting compounds that target viral factors which offer a lower risk of cytotoxicity but are plagued by a high risk of resistant mutant emergence, especially for RNA viruses with inherently high mutation rates. The use of combinatorial therapy may be able to offset this risk, but the design of specific viral targeting compounds principally limit their spectrum of activity[57], such as in the COVID-19 pandemic caused by SARS-CoV-2. We have shown using EV-A71, CHIKV, ZIKV, DENV2, SARS-CoV-2, MHV and HSV1 that broad-spectrum host-acting compounds, like peruvoside, are potent antivirals. As our understanding of host-pathogen interactions improves, broad-spectrum host-acting compounds could be developed as a viable and complementary strategy against fast evolving, emerging viral pathogens that may arise in future.

Acknowledgments

We would like to thank A/P Vincent T.K. Chow for kindly providing us with Echovirus 7 (Wallace), CV-A16 (G-10), EV-A71 (HFM41) and MHV (Strain A59), and Environment Health Institute (Singapore) for providing us with CHIKV (SGEHICHD 122508). This work was funded by Ministry of Education Tier 2 grant (MOE2017-T2-1-078 and MOE-2017-T2-2-014, Singapore) and National Research Foundation Competitive Research Programme (NRF-CRP21-2018-0004, Singapore). The funders had no role in study design, data collection and analysis, decision to publish, or preparation of the manuscript.

Author contributions

Justin Jang Hann Chu conceptualized the study. Kan Xing Wu and Thinesshwary Yogarajah performed the experiments and analyzed the data. Marcus Wing Choy Loe, Parveen Kaur, Regina Ching Hua Lee, Chee Keng Mok, Yi Hao Wong, Patchara Phuektes, and Li Sze Yeo performed the experiments. Kan Xing Wu, Thinesshwary Yogarajah, Yong Wah Tan, and Justin Jang Hann Chu wrote the paper. Kan Xing Wu and Thinesshwary Yogarajah are co-first authors. Justin Jang Hann Chu supervised the research. All of the authors have read and approved the final manuscript.

Conflicts of interest

The authors declare no competing interests.

Appendix A. Supporting information

Supporting data to this article can be found online at https://doi.org/10.1016/j.apsb.2023.03.015.

References

1. Wileman T, Netherton CL, Powell PP. Virus factories and mini-organelles generated for virus replication. *Encyclopedia of Cell Biology* 2016;**2**:819–27.
2. Wolff G, Melia CE, Snijder EJ, Barcena M. Double-membrane vesicles as platforms for viral replication. *Trends Microbiol* 2020;**28**:1022–33.
3. Poon LLM, Peiris M. Emergence of a novel human coronavirus threatening human health. *Nat Med* 2020;**26**:317–9.
4. Wu JT, Leung K, Bushman M, Kishore N, Niehus R, de Salazar PM, et al. Estimating clinical severity of COVID-19 from the transmission dynamics in Wuhan, China. *Nat Med* 2020;**26**:506–10.
5. Sandtner W, Egwolf B, Khalili-Araghi F, Sanchez-Rodriguez JE, Roux B, Bezanilla F, et al. Ouabain binding site in a functioning Na^+/K^+ ATPase. *J Biol Chem* 2011;**286**:38177–83.

6. Scheiner-Bobis G, Schoner W. A fresh facet for ouabain action. *Nat Med* 2001;**7**:1288−9.
7. Bagrov AY, Shapiro JI, Fedorova OV. Endogenous cardiotonic steroids: physiology, pharmacology, and novel therapeutic targets. *Pharmacol Rev* 2009;**61**:9−38.
8. Tian J, Cai T, Yuan Z, Wang H, Liu L, Haas M, et al. Binding of Src to Na^+/K^+-ATPase forms a functional signaling complex. *Mol Biol Cell* 2006;**17**:317−26.
9. Kometiani P, Li J, Gnudi L, Kahn BB, Askari A, Xie Z. Multiple signal transduction pathways link Na^+/K^+-ATPase to growth-related genes in cardiac myocytes. The roles of Ras and mitogen-activated protein kinases. *J Biol Chem* 1998;**273**:15249−56.
10. Xie Z, Kometiani P, Liu J, Li J, Shapiro JI, Askari A. Intracellular reactive oxygen species mediate the linkage of Na^+/K^+-ATPase to hypertrophy and its marker genes in cardiac myocytes. *J Biol Chem* 1999;**274**:19323−8.
11. Aizman O, Uhlen P, Lal M, Brismar H, Aperia A. Ouabain, a steroid hormone that signals with slow calcium oscillations. *Proc Natl Acad Sci U S A* 2001;**98**:13420−4.
12. Hoffmann HH, Palese P, Shaw ML. Modulation of influenza virus replication by alteration of sodium ion transport and protein kinase C activity. *Antiviral Res* 2008;**80**:124−34.
13. Bertol JW, Rigotto C, de Padua RM, Kreis W, Barardi CR, Braga FC, et al. Antiherpes activity of glucoevatromonoside, a cardenolide isolated from a Brazilian cultivar of *Digitalis lanata*. *Antiviral Res* 2011;**92**:73−80.
14. Su CT, Hsu JT, Hsieh HP, Lin PH, Chen TC, Kao CL, et al. Anti-HSV activity of digitoxin and its possible mechanisms. *Antiviral Res* 2008;**79**:62−70.
15. Cai H, Wang HY, Venkatadri R, Fu DX, Forman M, Bajaj SO, et al. Digitoxin analogues with improved anticytomegalovirus activity. *ACS Med Chem Lett* 2014;**5**:395−9.
16. Reed LJ, Muench H. A simple method of estimating fifty per cent endpoints. *Am J Epidemiol* 1938;**27**:493−7.
17. Low JS, Wu KX, Chen KC, Ng MM, Chu JJ. Narasin, a novel antiviral compound that blocks dengue virus protein expression. *Antivir Ther* 2011;**16**:1203−18.
18. Sun J, Yogarajah T, Lee RCH, Kaur P, Inoue M, Tan YW, et al. Drug repurposing of pyrimidine analogs as potent antiviral compounds against human enterovirus A71 infection with potential clinical applications. *Sci Rep* 2020;**10**:8159.
19. Burns CC, Lawson MA, Semler BL, Ehrenfeld E. Effects of mutations in poliovirus 3Dpol on RNA polymerase activity and on polyprotein cleavage. *J Virol* 1989;**63**:4866−74.
20. Carpenter AE, Jones TR, Lamprecht MR, Clarke C, Kang IH, Friman O, et al. CellProfiler: image analysis software for identifying and quantifying cell phenotypes. *Genome Biol* 2006;**7**:R100.
21. Tan YW, Yam WK, Sun J, Chu JJH. An evaluation of chloroquine as a broad-acting antiviral against hand, foot and mouth disease. *Antiviral Res* 2018;**149**:143−9.
22. Prassas I, Diamandis EP. Novel therapeutic applications of cardiac glycosides. *Nat Rev Drug Discov* 2008;**7**:926−35.
23. McGarry SJ, Williams AJ. Digoxin activates sarcoplasmic reticulum Ca^{2+}-release channels: a possible role in cardiac inotropy. *Br J Pharmacol* 1993;**108**:1043−50.
24. Mekahli D, Bultynck G, Parys JB, De Smedt H, Missiaen L. Endoplasmic-reticulum calcium depletion and disease. *Cold Spring Harb Perspect Biol* 2011;**3**:a004317.
25. He B. Viruses, endoplasmic reticulum stress, and interferon responses. *Cell Death Differ* 2006;**13**:393−403.
26. Samali A, Fitzgerald U, Deegan S, Gupta S. Methods for monitoring endoplasmic reticulum stress and the unfolded protein response. *Int J Cell Biol* 2010;**2010**:830307.
27. Nagy PD, Strating JR, van Kuppeveld FJ. Building viral replication organelles: close encounters of the membrane types. *PLoS Pathog* 2016;**12**:e1005912.
28. Miller S, Krijnse-Locker J. Modification of intracellular membrane structures for virus replication. *Nat Rev Microbiol* 2008;**6**:363−74.
29. Jackson WT. Poliovirus-induced changes in cellular membranes throughout infection. *Curr Opin Virol* 2014;**9**:67−73.
30. Wang J, Wu Z, Jin Q. COPI is required for enterovirus 71 replication. *PLoS One* 2012;**7**:e38035.
31. Fujiwara T, Oda K, Yokota S, Takatsuki A, Ikehara Y. Brefeldin A causes disassembly of the Golgi complex and accumulation of secretory proteins in the endoplasmic reticulum. *J Biol Chem* 1988;**263**:18545−52.
32. Iglesias NG, Mondotte JA, Byk LA, De Maio FA, Samsa MM, Alvarez C, et al. Dengue virus uses a non-canonical function of the host GBF1−Arf−COPI system for capsid protein accumulation on lipid droplets. *Traffic* 2015;**16**:962−77.
33. Zhang N, Zhang L. Key components of COPI and COPII machineries are required for chikungunya virus replication. *Biochem Biophys Res Commun* 2017;**493**:1190−6.
34. Morohashi Y, Balklava Z, Ball M, Hughes H, Lowe M. Phosphorylation and membrane dissociation of the ARF exchange factor GBF1 in mitosis. *Biochem J* 2010;**427**:401−12.
35. Mao L, Li N, Guo Y, Xu X, Gao L, Xu Y, et al. AMPK phosphorylates GBF1 for mitotic Golgi disassembly. *J Cell Sci* 2013;**126**:1498−505.
36. Delang L, Paeshuyse J, Neyts J. The role of phosphatidylinositol 4-kinases and phosphatidylinositol 4-phosphate during viral replication. *Biochem Pharmacol* 2012;**84**:1400−8.
37. de Wilde AH, Wannee KF, Scholte FE, Goeman JJ, Ten Dijke P, Snijder EJ, et al. A kinome-wide small interfering RNA screen identifies proviral and antiviral host factors in severe acute respiratory syndrome coronavirus replication, including double-stranded RNA-activated protein kinase and early secretory pathway proteins. *J Virol* 2015;**89**:8318−33.
38. Horiuchi M, Kuga T, Saito Y, Nagano M, Adachi J, Tomonaga T, et al. The tyrosine kinase v-Src causes mitotic slippage by phosphorylating an inhibitory tyrosine residue of Cdk1. *J Biol Chem* 2018;**293**:15524−37.
39. Jackson CL. Activators and effectors of the small G protein Arf1 in regulation of golgi dynamics during the cell division cycle. *Front Cell Dev Biol* 2018;**6**:29.
40. Romero-Brey I, Bartenschlager R. Membranous replication factories induced by plus-strand RNA viruses. *Viruses* 2014;**6**:2826−57.
41. Heaton NS, Randall G. Dengue virus-induced autophagy regulates lipid metabolism. *Cell Host Microbe* 2010;**8**:422−32.
42. Egger D, Teterina N, Ehrenfeld E, Bienz K. Formation of the poliovirus replication complex requires coupled viral translation, vesicle production, and viral RNA synthesis. *J Virol* 2000;**74**:6570−80.
43. Whetsell WO Jr, Bunge RP. Reversible alterations in the Golgi complex of cultured neurons treated with an inhibitor of active Na and K transport. *J Cell Biol* 1969;**42**:490−500.
44. Schmitt JM, Wayman GA, Nozaki N, Soderling TR. Calcium activation of ERK mediated by calmodulin kinase I. *J Biol Chem* 2004;**279**:24064−72.
45. Johnston BP, McCormick C. Herpesviruses and the unfolded protein response. *Viruses* 2019;**12**:17.
46. Carafoli E. Calcium signaling: a tale for all seasons. *Proc Natl Acad Sci U S A* 2002;**99**:1115−22.
47. Agirre A, Barco A, Carrasco L, Nieva JL. Viroporin-mediated membrane permeabilization. Pore formation by nonstructural poliovirus 2B protein. *J Biol Chem* 2002;**277**:40434−41.
48. Hyser JM, Collinson-Pautz MR, Utama B, Estes MK. Rotavirus disrupts calcium homeostasis by NSP4 viroporin activity. *mBio* 2010;**1**.002655-e310.
49. Wang J, Hu Y, Zheng M. Enterovirus A71 antivirals: past, present, and future. *Acta Pharm Sin B* 2022;**12**:1542−66.
50. Tang D, Mar K, Warren G, Wang Y. Molecular mechanism of mitotic Golgi disassembly and reassembly revealed by a defined reconstitution assay. *J Biol Chem* 2008;**283**:6085−94.
51. Savidis G, McDougall WM, Meraner P, Perreira JM, Portmann JM, Trincucci G, et al. Identification of zika virus and dengue virus dependency factors using functional genomics. *Cell Rep* 2016;**16**:232−46.
52. Verheije MH, Raaben M, Mari M, Te Lintelo EG, Reggiori F, van Kuppeveld FJ, et al. Mouse hepatitis coronavirus RNA replication

depends on GBF1-mediated ARF1 activation. *PLoS Pathog* 2008;**4**: e1000088.
53. Zhou X, Zhu L, Bondy C, Wang J, Luo Q, Chen Y. AG1478 elicits a novel anti-influenza function *via* an EGFR-independent, GBF1-dependent pathway. *Int J Mol Sci* 2022;**23**:5557.
54. Zhao X, Claude A, Chun J, Shields DJ, Presley JF, Melancon P. GBF1, a *cis*-Golgi and VTCs-localized ARF-GEF, is implicated in ER-to-Golgi protein traffic. *J Cell Sci* 2006;**119**:3743−53.
55. Zhang L, Hong Z, Lin W, Shao RX, Goto K, Hsu VW, et al. ARF1 and GBF1 generate a PI4P-enriched environment supportive of hepatitis C virus replication. *PLoS One* 2012;**7**:e32135.
56. Solignat M, Gay B, Higgs S, Briant L, Devaux C. Replication cycle of chikungunya: a re-emerging arbovirus. *Virology* 2009;**393**:183−97.
57. Martinez JP, Sasse F, Bronstrup M, Diez J, Meyerhans A. Antiviral drug discovery: broad-spectrum drugs from nature. *Nat Prod Rep* 2015;**32**:29−48.